ELSEVIER

Contents lists available at ScienceDirect

International Journal of Thermofluids

journal homepage: www.elsevier.com/locate/ijtf



A semi-analytical analysis on transfer behaviour of heat and mass on the viscous dissipated MHD UCM fluid flow between squeezing plates

Pareekshith G. Bhat a, Ali J. Chamkha b, Nityanand P. Pai c, Sampath Kumar V.S. a,*

- ^a Department of Mathematics, Manipal Institute of Technology, Manipal Academy of Higher Education, Manipal, 576104, Karnataka, India
- b Faculty of Engineering, Kuwait College of Science and Technology, Doha District, 35005, Al Asimah Governate, Kuwait
- ^c Department of Mathematics, NMAM Institute of Technology (Nitte Deemed to be University), Nitte, Karkala, Udupi, 574110, Karnataka, India

ARTICLE INFO

Keywords: Upper convected Maxwell fluid Viscous dissipation Heat transfer Thermal radiation Mass transfer Homotopy perturbation method

ABSTRACT

The current study strives to theoretically examine the heat and mass transfer properties on the magnetohy-drodynamic upper convected Maxwell fluid flow through a squeezing channel of parallel plates. Due to its vast applications, such as lubrication systems and bearing, the flow of upper convected Maxwell fluid through the channel comprising a moving impermeable top plate and a stationary porous bottom that is responsible for injection and suction effects in addition to squeezing motion is analysed in the study. The fundamental equations governing the conservation laws of fluid mechanics are transfigured into a non-linear system of ordinary differential equations adopting similarity transformations along with the boundary conditions. The so-obtained non-linear ordinary differential equations are then approached by the homotopy perturbation method to achieve an approximate analytic solution. Various graphs concerning the velocity, temporal, and concentration profiles are plotted against distinct pertinent parameters that pose a physical impact on the model. It is observed that the temporal distribution field elevates with a rise in the Eckert number and a decrease in the radiation parameter. Further, it is noticed that the concentration profile upsurges with a hike in the radiation parameter and depletion in the Eckert number. Moreover, the numerical values corresponding to the coefficient of skin friction, and rates of heat and mass transfer are tabulated for distinct pertinent parameters involved in the study.

1. Introduction

In today's world, science and technology are rapidly developing with an increasing demand for modernity and industries. Most of these science and technological fields are dependent on the flow and transfer phenomena that arise in the motion of fluids. Thus, the concept of fluids in motion has bloomed in such a way that it has become one of the essentials in everyday life. Due to such advancements in daily needs, researchers find it one of the most exciting and also extremely challenging fields in the current scenario. In the present day, fluid mechanics turns out to be one of the pillars for advancement in various fields such as mechanical, chemical, aeronautical engineering, and many more. Though the study of fluids first started with Archimedes [1] back in 250 BC, the theoretical analysis of the fluids in motion came into existence in the latter half of the 18th century. With an increasing demand for goods, the experimental analysis of any situation is considered to be laborious, time-consuming, and cost-inefficient. Hence, the theoretical analysis is essential prior to the experimental findings. Thus, mathematical modelling of the physical situation has found its significance.

The study on the flow of fluid across a channel made up of infinitely long plates placed parallel is one of the significant domains in fluid mechanics that drives numerous applications across various scientific and industrial arenas. The reason for the notable importance of this field is due to its diverse applications that are handy in understanding the fundamentals of fluid dynamics, developing microfluidic devices, industrial processes, heat transfer technology enhancement, geological and environmental insights, designing aerospace and automotive, and many more. Altogether, the theoretical analysis of fluid flow between plates, in addition to providing insights into a wide range of applications, it underpins the theoretical groundwork for the advancement of fluid dynamics and its applications across various disciplines. Further, the fluid flow between moving plates or simply the fluid flow between squeezing plates has revolutionized the applications in chemistry, specifically in microfluidic devices. Moreover, the squeezing flow finds varied applications in lubrication technology, the automotive sector, and many more. In totality, the analysis of fluid squeezed between a pair of parallel plates is vital across multiple disciplines for both theoretical knowledge as well as practical applications. Furthermore,

E-mail address: sampath.kvs@manipal.edu (Sampath Kumar V.S.).

https://doi.org/10.1016/j.ijft.2025.101202

Received 24 January 2025; Received in revised form 1 April 2025; Accepted 1 April 2025 Available online 15 April 2025

^{*} Corresponding author.

it lays the foundation for developing solutions to various real-world problems and is one of the keys to the advancement of technology in various sectors.

The flow of fluid between porous parallel plates, often referred to as flow through porous media, is a critical aspect of several fields of science and engineering, mainly comprising hydro-geology, petrochemical, civil, and environmental engineering. This concept is very crucial in understanding the flow of groundwater through porous layers of soil and rocks, the recovery of oil and gas, the extraction of geothermal energy, evaluating the stability and durability of a structure, movement of pollutants through the ground, irrigation and drainage, and many more. In summary, the study of fluid flowing past a porous medium is fundamental in addressing a wide range of practical problems related to various fluid resource management and many other fields. Hamza [2] examined the repercussions of injection and suction on the flow of an incompressible viscous fluid betwixt two plates placed parallelly. The sequel of fluid inertia on the viscous fluid flowing axisymmetrically between two massive moving plates resulting in a squeezing motion was theoretically investigated by Ghori et al. [3]. Further, Khan et al. [4] examined theoretically the fluid flow squeezed through a channel comprising two infinitely long plates parallel to each other with special reference to Casson fluid. Several other researchers have analysed the flow of fluid through porous media in the recent past [5,6].

Nomenclature	
τ	Cauchy stress tensor (in Pa)
S	extra stress tensor (in Pa)
μ	dynamic viscosity (in Pas)
λ	relaxation time (in s)
A_1	Rivlin–Ericksen tensor (in Pa)
h	distance between the plates (in m)
ρ	fluid density (in kgm ⁻³)
p	pressure (in Pa)
u	x- directional velocity (in ms ⁻¹)
v	y-directional velocity (in ms ⁻¹)
ν	kinematic viscosity (in m ² s ⁻¹)
σ	electrical conductivity (in Sm ⁻¹)
B_0	uniform magnetic field applied along y- direction
	(in T)
k	porous media's permeability (in m ²)
ω	porosity (dimensionless)
k_0	thermal conductivity (in Wm ⁻¹ K ⁻¹)
q_{rad}	radiation heat flux (in Wm ⁻²)
T	temperature of the system (in K)
C_P	specific heat capacity (in Jkg ⁻¹ kg ⁻¹ K ⁻¹)
k^*	mean absorption coefficient (in m ⁻¹)
σ^*	Stefan–Boltzmann constant (in Wm ⁻² K ⁻⁴)
T_1	lower plate's temperature (in K)
T_2	upper plate's temperature (in K)
D_B	coefficient of Brownian motion (in m ² s ⁻¹)
D_T	Thermophoretic diffusion (in m ² s ⁻¹)
k_1	first-order chemical reaction rate (in s ⁻¹)
C	fluid concentration (in kgm ⁻³)
C_1	lower plate's concentration (in kgm ⁻³)
C_2	upper plate's concentration (in kgm ⁻³)
V_h	upper plate's velocity in y - direction (in kgm ⁻³)
A	injection/suction parameter (in ms ⁻¹)

In physics, magneto-hydrodynamics (MHD) is the study of the dynamics of electrically conducting fluids. The study of the magnetic field's influence on the fluid and the magnetic field generated by the movement of fluids are the key principles of MHD. Capitalizing on how the magnetic field interacts with the electrically conducting fluids, MHD encompasses an exceptional range of potential revolutionary applications in various fields such as fusion energy, metallurgy, power

generation, material processing, aerospace and propulsion, environmental engineering, biomedical, geophysics, and many more. Thus, it is crucial to analyse the interplay of this interdisciplinary field that merges the concepts of fluid dynamics with electromagnetism in order to manipulate and analyse fluid flows. Hughes et al. [7] initially investigated the movement of an incompressible electrically conducting viscous fluid flowing betwixt parallel rotating disks under the impact of a magnetic field applied externally and coining it as MHD. The impacts of fluid inertia and buoyant forces on the fluid flow between squeezing films in the existence of a magnetic field that is applied externally were both experimentally and theoretically analysed by Kuzma et al. [8]. Several other authors have analysed the impact of MHD in various fluid flows [9–14].

Heat transfer analysis arising in fluid flow is fundamental for design, safety, efficiency, and innovation in various industries that contribute to the advancement of technology. Also, analysis of heat transfer is crucial for several reasons that intersect with both theoretical understanding and engineering applications such as cooling and heating systems, power generation, electronics cooling, refrigeration and freezing, renewable energy systems, climate control, material and chemical processing, and many more. Moreover, the applications of heat transfer are diversified even into medical fields such as hyperthermia treatment, cryotherapy, medical imaging, and a lot more. Therefore understanding the principle of heat transfer is essential in optimizing these processes, improving energy efficiency, and further developing innovative solutions to technical challenges. Kim [15] theoretically studied the unsteady two-dimensional heat transfer on the laminar flow of an incompressible electrically conducting viscous fluid past a vertical semi-infinite porous plate with variable suction. Cortell [16] numerically analysed the heat transfer behaviour on an incompressible fluid flow past moving parallel sheets. Various other researchers have theoretically analysed the heat transfer properties on fluid flow in the past [17-24].

The analysis of thermal radiation plays a vital role in having a better understanding of the heat transfer processes because, unlike convection and conduction, thermal radiation is capable of transferring heat without any medium. Also, thermal radiation aids in designing and analysing thermal management systems where radiative heat transfer is predominant, and in designing cooling systems for electronic devices that require efficient heat management for performance and longevity. Thus, the study of thermal radiation in fluid flow is ever interesting due to its role in heat transfer, system design, and optimization. Chamkha [25] theoretically investigated the repercussions of thermal radiation on the characteristics of flow and heat transfer of the fluid past a surface with the existence of a gravitational field. Das [26] analysed theoretically the effect of thermal radiation on the characteristics of heat transfer in the hydromagnetic fluid flow over a flat plate considering convective surface heat flux at the boundary and heat source/sink. Numerous other researchers have also analysed this effect on various fluid flows between plates in the past [27-30].

The movement of substances from one phase to another within a fluid that is flowing is known as mass transfer. This phenomenon is incredibly impactful with numerous industrial applications such as biotechnology, and chemical and environmental engineering. These industrial applications encompass various robust processes such as distillation, absorption, extraction, wastewater treatment, air pollution control, and many more. Thus, a deeper understanding of this phenomenon is essential in optimizing industrial processes and designing more efficient systems that are capable of transferring substances between different phases within the fluid. Makinde [31] analysed theoretically the heat and mass transfer characteristics on the MHD boundary layer flow over a drifting vertical plate with convective surface boundary conditions. Singh et al. [32] conducted an unsteady two-dimensional analysis on the heat and mass transfer properties of the nanofluid that is made to flow between a pair of parallel plates with

an applied magnetic field. Several other researchers have also analysed the mass transfer characteristics in the past [33–39].

The fluids are broadly categorized as Newtonian and non-Newtonian depending on the Newton's law of viscosity. This study mainly focuses on the non-Newtonian fluid that is categorized under the rate type of fluid specifically the Maxwell fluid [40]. In recent days, the Maxwell fluid has gained prominence due it its unique properties that allow it to flow and deform under stress making it the best choice for reducing damping and frictional vibration. The Maxwell fluids because of their reliability have robust applications in various technical and industrial fields such as designing and construction and further developing hydraulic systems, shock absorbers, and lubrication systems.

The rheological model that well describes the behaviour of viscoelastic fluids is the upper convected Maxwell (UCM) fluid model which takes into account both elastic and viscous effects as a response to the stress and deformation of the fluid. Further, the visco-elastic behaviour of the fluid is governed by the relaxation and retardation time that characterize the UCM model. The UCM fluid model is widely used in the analysis of the flow of non-Newtonian fluids and has been found to have various applications in various scientific and engineering arenas such as polymer processing, food manufacturing, blood pumps, drug delivery, extrusion, injection moulding, coating process, geophysics, petroleum and geotechnical engineering, and many more. Additionally, several solutions containing high molecular weight polymers exhibit UCM behaviour such as acrylic and polyethylene oxide. Fluids like mucus and toothpaste also exhibit the UCM fluid model.

Abbas et al. [41] examined the two-dimensional MHD boundary layer flow of the UCM fluid through a porous channel. The impact of thermal radiation on the Maxwell fluid flow through a porous channel in the presence of an applied magnetic field was analysed by Hayat et al. [42]. Ojjela et al. [43] studied theoretically the influence of Hall and ion slip currents on the heat transfer characteristics of chemically reacting UCM fluid that is flowing through a porous channel. Further, UCM fluid flow through a channel comprising of a moving and stationary porous plate was theoretically investigated by Pai et al. [44]. Several other authors have studied the Maxwell fluid flow in the past [45–51].

From the literature, it was observed that the impact of chemical reaction on the viscous dissipated heat and mass transfer of MHD UCM fluid flow with the influence of thermal radiation has numerous practical applications in various technical and industrial arenas. Furthermore, conducting direct experimental analysis can prove to be laborious, time-consuming, and cost inefficient resulting in an alternate feasible technique. Thus, theoretical analysis on the properties of heat and mass transfer of such fluid flows is crucial in obtaining a broader perspective. Moreover, the authors found it necessary to investigate theoretically the heat and mass transfer properties on the UCM fluid flow betwixt a pair of infinitely long parallel porous squeezing plates as the studies on UCM fluids were limited in the past due to the complexities involved. Thus, this study aims to fill this gap with the intent of further advancement in the scientific domain.

Most of the real-world problems are mathematically modelled with the help of differential equations. It is necessary to solve the so obtained mathematical equations with specified boundary conditions once the physical problem is successfully formulated. Due to the non-linearity in nature, the resulting mathematical equations turn out to be highly non-linear. As a result, analytical solutions to such equations are nearly impossible with the existing knowledge. Thus, computational methods are employed to handle such equations which are highly non-linear. Researchers face several challenges in obtaining approximate solutions using numerical methods. In order to tackle the challenges obtained in these techniques, researchers came up with semi-analytical techniques to obtain approximate solutions. One such prominent semi-analytical method that is capable of yielding better results to non-linear differential equations arising in nature is the Homotopy perturbation method (HPM). Initially proposed by He [52] in 1999, HPM can be applied

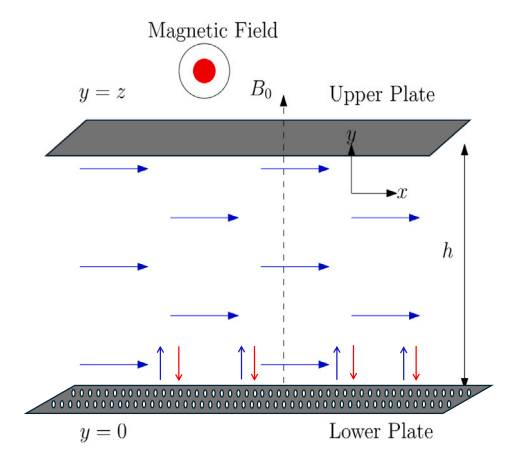


Fig. 1. Schematic representation of the Flow.

efficiently and conveniently in achieving better and more accurate solutions [53,54]. Further, Babolian et al. [55] illustrated the global homotopy equation to solve non-linear differential equations. Additionally, because HPM is underpinned by power series, it preserves the analytic structure of the solution, making it an excellent choice for researchers. Furthermore, its rapid convergence makes HPM more advantageous compared to other methods. Moreover, a single computer program can provide solutions for extensive expansions instead of just a single term, due to which, it can be noted that HPM can produce results with minimal computational effort. Numerous other authors have employed semi-analytical methods to obtain better approximations in the recent past [56–60].

The existing literature highlights a significant gap in the study of heat and mass transfer properties influenced by viscous dissipation and thermal radiation in the MHD squeezing flow of UCM fluids, primarily due to the fluid's intricate behaviour. Despite this challenge, UCM fluids possess a wide range of industrial and engineering applications, including lubrication, hydraulics, and various other complex systems. Thus, the current study intends to theoretically analyse the chemical reaction and thermal radiation impacts on the behaviour of viscous dissipated heat and mass transfer arising in the UCM fluid flow squeezed betwixt infinitely long parallel porous plates considering that the magnetic field is applied externally. In the present study, the top plate is considered to impermeable and approaching or departing from the stationary porous lower plates. Further, in order to achieve a better approximate solution, HPM is employed to solve the arising ordinary differential equations (ODEs) after adopting a suitable similarity transformation. The graphs concerning the velocity distributions, temperature fields, and concentration profiles are plotted against various pertinent physical parameters arising in the problem. Moreover, the numerical values associated with the skin friction coefficient, and rates of heat and mass transfer are tabulated.

2. Mathematical formulation

Consider the steady viscous incompressible MHD flow of a UCM fluid along a two-dimensional channel formed by a porous stationary bottom plate and a moving impermeable top plate with the influence of thermal radiation as shown in Fig. 1.

The rheological equations that constitute the UCM fluid is given by [61],

$$\tau = -PI + S,\tag{1}$$

where

$$S + \lambda \left(\frac{dS}{dt} - LS - SL^{T}\right) = \mu A_{1}.$$
 (2)

Further.

$$A_1 = \nabla V + (\nabla V)^T \tag{3}$$

The elementary equations that govern the momentum, energy and chemical reaction of the UCM fluid flow are given by [33,35,42,45–47],

$$\frac{\partial u}{\partial x} + \frac{\partial v}{\partial y} = 0,\tag{4}$$

$$u\frac{\partial u}{\partial x} + v\frac{\partial u}{\partial y} + \lambda \left[u^2 \frac{\partial^2 u}{\partial x^2} + v^2 \frac{\partial^2 u}{\partial y^2} + 2uv \frac{\partial^2 u}{\partial x \partial y} \right] = -\frac{1}{\rho} \frac{\partial P}{\partial x} + v \left(\frac{\partial^2 u}{\partial x^2} + \frac{\partial^2 u}{\partial y^2} \right) - \frac{\sigma B_0^2}{\rho} \left(u + \lambda v \frac{\partial u}{\partial y} \right) - \frac{\omega v}{k} u,$$
 (5)

$$u\frac{\partial v}{\partial x} + v\frac{\partial v}{\partial y} + \lambda \left[u^2 \frac{\partial^2 v}{\partial x^2} + v^2 \frac{\partial^2 v}{\partial y^2} + 2uv \frac{\partial^2 v}{\partial x \partial y} \right] = -\frac{1}{\rho} \frac{\partial P}{\partial y} + v \left(\frac{\partial^2 v}{\partial x^2} + \frac{\partial^2 v}{\partial y^2} \right), \tag{6}$$

$$\rho C_P \left(u \frac{\partial T}{\partial x} + v \frac{\partial T}{\partial y} \right) = k_0 \left(\frac{\partial^2 T}{\partial x^2} + \frac{\partial^2 T}{\partial y^2} \right) - \frac{\partial q_{rad}}{\partial y} + \mu \left(\frac{\partial v}{\partial x} - \frac{\partial u}{\partial y} \right)^2, \tag{7}$$

$$u\frac{\partial C}{\partial x} + v\frac{\partial C}{\partial y} = D_B \left(\frac{\partial^2 C}{\partial x^2} + \frac{\partial^2 C}{\partial y^2}\right) + \frac{D_T}{T_1} \left(\frac{\partial^2 T}{\partial x^2} + \frac{\partial^2 T}{\partial y^2}\right) -k_1(C - C_1),\tag{8}$$

along with the boundary conditions specified as,

$$u = 0, \quad v = AV_h, \quad T = T_1, \quad C = C_1 \quad at \quad y = 0$$
 (9)

$$u = 0, \quad v = V_h, \quad T = T_2, \quad C = C_2 \quad at \quad y = h$$
 (10)

Here, u=0 implies no slip condition at both lower and upper plates. Further, it can be inferred from the conditions that the lower plate is considered to be porous through which the fluid is injected or sucked at a velocity AV_h and the upper plate moves towards and away from the lower at a constant velocity V_h . Moreover, the two plates are considered to be placed at different temperatures and concentrations respectively.

By Rosseland approximation for radiation [62],

$$q_{rad} = -\frac{4\sigma^*}{3k^*} \frac{\partial T^4}{\partial \nu}.\tag{11}$$

Adopting the Taylor's series expansion around T_1 ,

$$T^4 \cong 4T_1^3 T - 3T_1^4. \tag{12}$$

By adopting the following similarity transformations [42],

$$\xi = \frac{x}{h}, \qquad \eta = \frac{y}{h},$$

$$u = -V_h \xi F'(\eta), \qquad v = V_h F(\eta)$$

$$\theta(\eta) = \frac{T - T_1}{T_2 - T_1}, \qquad \phi(\eta) = \frac{C - C_1}{C_2 - C_1},$$

$$(13)$$

Eq. (5)–(8) transform into

$$F^{IV}(\eta) + R[F'(\eta)F''(\eta) - F(\eta)F'''(\eta)]$$

$$- M[RF''(\eta) + De[F'(\eta)F''(\eta) + F(\eta)F'''(\eta)]]$$

$$+ De[2F''(\eta)[F(\eta)(F''(\eta)) + (F'(\eta))^{2}]$$

$$+ (F(\eta))^{2}F^{IV}(\eta)] - KF''(\eta) = 0,$$
(14)

$$\left(1 + \frac{4}{3}Rd\right)G''(\eta) - Pr[RF(\eta)G'(\eta) - Ec(F''(\eta))^2] = 0,$$
(15)

$$H''(\eta) + \frac{N_T}{N_R}G''(\eta) - Sc[RF(\eta)H'(\eta) + KrH(\eta)] = 0.$$
 (16)

The relevant boundary conditions corresponding to the governing equations are therefore reduced into

$$F'(0) = 0$$
, $F(0) = A$, $G(0) = 0$, $H(0) = 0$, (17)

$$F'(1) = 0$$
, $F(1) = 1$, $G(1) = 1$, $H(1) = 1$. (18)

Moreover, the interested physical quantities in this study are the skin friction coefficient C_f , the rate of heat transfer Nu and the rate mass transfer Sh are respectively defined by

$$C_f = \frac{\mu\left(\frac{\partial u}{\partial y}\right)}{\rho V_h^2}, \quad Nu = \frac{-h\left(\frac{\partial T}{\partial y}\right)}{T_2 - T_1}, \quad Sh = \frac{-h\left(\frac{\partial C}{\partial y}\right)}{C_2 - C_1}.$$
 (19)

3. Mathematical solution

It is essential to solve the implied physical problem once it is successfully modelled with the relevant boundary conditions. The analytical solution to the considered problem is cumbersome due to the problem's non-linearity. Thus, computational methods are reliable in yielding approximate solutions to the concerning problem. In this study, a semi-analytical approach, specifically HPM, is adopted to plot various graphs related to velocity fields, temperature distribution curves, and concentration profiles. Further, the numerical values associated with coefficient of skin friction, and rates of heat and mass transfer are numerically tabulated.

3.1. Homotopy perturbation method:

In the current analysis, three non-linear ODEs are obtained, one fourth order and two second order, that correspond to momentum, energy, and chemical reaction equations respectively. These mathematical equations are approached by HPM in the following manner:

Let A_i represent the differential operator acting on unknown functions $f(\chi)$ with the known functions denoted by $f_i(\chi)$. The equations in the considered problem can be thus represented as

$$A_i[f(\chi)] - f_i(\chi) = 0.$$
 (20)

In HPM, generally the operator A_i is put forth as sum of one linear part and another non-linear,

$$A_i = L_i + R_i, (21)$$

where the linear and the remaining part of A_i is denoted by L_i and R_i respectively.

Further, by choosing L_i and initial guess v_0 wisely from Eqs. (14)–(16) and the boundary conditions specified in Eqs. (17) and (18) respectively, the homotopy equation corresponding to Eq. (20) is constructed in the following manner:

$$H_i(\chi_i, p) = L_i(\chi_i, p) - L_i(v_0(\eta)) + p[R_i(\chi_i, p) - f_i(\chi_i) + L_i(v_0(\eta))] = 0, (22)$$

where i = 1, 2, 3

The solution of Eq. (22) is assumed to be in the form of power series,

$$\chi_i(\eta, p) = \sum_{n=0}^{\infty} p^n f_n(\eta). \tag{23}$$

Solution to the considered problem is Eq. (23) when p = 1.

By adopting the above mentioned procedure of HPM, the initial three terms of the solutions to the non-linear ordinary differential equations are obtained as given below:

$$F_0(\eta) = 2A\eta^3 - 3A^2 + A - 2\eta^3 + 3\eta^2 \tag{24}$$

$$G_0(\eta) = \eta \tag{25}$$

$$H_0(\eta) = \eta \tag{26}$$

$$\begin{split} F_1(\eta) &= \frac{1}{420} (-200A^3De\eta^9 + 900A^3De\eta^8 - 1368A^3De\eta^7 \\ &+ 420A^3De\eta^6 + 1008A^3De\eta^5 - 1260A^3De\eta^4 \\ &+ 656A^3De\eta^3 - 156A^3De\eta^2 - 48A^2MDe\eta^7 \\ &+ 168A^2MDe\eta^6 - 126A^2MDe\eta^5 - 210A^2MDe\eta^4 \\ &+ 366A^2MDe\eta^3 - 150A^2MDe\eta^2 - 24A^2R\eta^7 \\ &+ 84A^2R\eta^6 - 126A^2R\eta^5 + 210A^2R\eta^4 - 258A^2R\eta^3 \\ &+ 114A^2R\eta^2 + 600A^2De\eta^9 - 2700A^2De\eta^8 \\ &+ 4104A^2De\eta^7 - 1596A^2De\eta^6 - 2016A^2De\eta^5 \\ &+ 2520A^2De\eta^4 - 1128A^2De\eta^3 + 216A^2De\eta^2 \\ &+ 42AK\eta^5 - 105AK\eta^4 + 84AK\eta^3 - 21AL\eta^2 \\ &+ 42AMR\eta^5 - 105AMR\eta^4 + 84AMR\eta^3 - 21AMR\eta^2 \\ &+ 96AMDe\eta^7 - 336AMDe\eta^6 + 252AMDe\eta^5 + \cdots) \end{split}$$

$$G_{1}(\eta) = -\frac{3}{20(4Rd+3)}(240A^{2}EcPr\eta^{4} - 480A^{2}EcPr\eta^{3} + 360A^{2}EcPr\eta^{2} - 120A^{2}EcPr\eta - 480AEcPr\eta^{4} + 960AEcPr\eta^{3} - 720AEcPr\eta^{2} + 240AEcPr\eta - 2APrR\eta^{5} + 5APrR\eta^{4} - 10APrR\eta^{2} + 7APrR\eta + 240EcPr\eta^{4} - 480EcPr\eta^{3} + 360EcPr\eta^{2} - 120EcPr\eta + 2PrR\eta^{5} - 5PrR\eta^{4} + 3PrR\eta)$$
(28)

$$H_1(\eta) = \frac{1}{60} (6ARSc\eta^5 - 15ARSc\eta^4 + 30ARSc\eta^2 - 21ARSc\eta - 6RSc\eta^5 + 15RSc\eta^4 - 9RSc\eta - 10Sc\eta^3Kr + 10Sc\eta Kr)$$
(29)

$$\begin{split} F_2(\eta) &= \frac{1}{8408400} (352000 A^5 D e^2 \eta^{15} - 1760000 A^4 D e^2 \eta^{15} \\ &+ 3520000 A^3 D e^2 \eta^{15} - 3520000 A^2 D e^2 \eta^{15} \\ &+ 1760000 A D e^2 \eta^{15} - 352000 D e^2 \eta^{15} \\ &- 2640000 A^5 D e^2 \eta^{14} + 13200000 A^4 D e^2 \eta^{14} \\ &- 26400000 A^3 D e^2 \eta^{14} + 26400000 A^2 D e^2 \eta^{14} \\ &- 13200000 A D e^2 \eta^{14} + 2640000 D e^2 \eta^{14} \\ &+ 8484000 A^5 D e^2 \eta^{13} - 42420000 A^4 D e^2 \eta^{13} \\ &+ 84840000 A^3 D e^2 \eta^{13} - 84840000 A^2 D e^2 \eta^{13} \\ &+ 42420000 A D e^2 \eta^{13} + 700000 A^4 M D e^2 \eta^{13} \\ &- 2800000 A^3 M D e^2 \eta^{13} + 4200000 A^2 M D e^2 \eta^{13} \\ &- 2800000 A M D e^2 \eta^{13} + 700000 M D e^2 \eta^{13} \\ &- 8484000 D e^2 \eta^{13} + 56000 A^4 R D e \eta^{13} + \cdots) \end{split}$$

$$\begin{split} G_2(\eta) &= \frac{1}{92400(4Rd+3)^2} (-3600A^3PrRDe\eta^{11} \\ &+ 10800A^2PrRDe\eta^{11} - 10800APrRDe\eta^{11} \\ &+ 3600PrRDe\eta^{11} - 4800A^3PrRdRDe\eta^{11} \\ &+ 14400A^2PrRdRDe\eta^{11} - 14400APrRdRDe\eta^{11} \\ &+ 14400A^2PrRdRDe\eta^{11} + 7603200A^4EcPrDe\eta^{10} \\ &- 30412800A^3EcPrDe\eta^{10} + 45619200A^2EcPrDe\eta^{10} \\ &- 30412800AEcPrDe\eta^{10} + 7603200EcPrDe\eta^{10} \\ &+ 10137600A^4EcPrRdDe\eta^{10} \\ &- 40550400A^3EcPrRdDe\eta^{10} \\ &+ 60825600A^2EcPrRdDe\eta^{10} \\ &- 40550400AEcPrRdDe\eta^{10} \\ &+ 10137600EcPrRdDe\eta^{10} \\ &+ 10137600EcPrRdDe\eta^{10} \\ \end{split}$$

 $H_2(\eta) = \frac{1}{277200 N_B (4Rd + 3)} (-3600 A^3 N_B RSc De \eta^{11}$

$$\begin{split} &+ 10800A^2N_BRScDe\eta^{11} - 10800AN_BRScDe\eta^{11} \\ &+ 3600N_BRScDe\eta^{11} - 4800A^3N_BRdRScDe\eta^{11} \\ &+ 14400A^2N_BRdRScDe\eta^{11} - 14400AN_BRdRScDe\eta^{11} \\ &+ 14800N_BRdRScDe\eta^{11} + 19800A^3N_BRScDe\eta^{10} \\ &+ 59400A^2N_BRScDe\eta^{10} + 59400AN_BRScDe\eta^{10} \\ &- 59400A^2N_BRScDe\eta^{10} + 26400A^3N_BRdRScDe\eta^{10} \\ &- 19800N_BRScDe\eta^{10} + 26400A^3N_BRdRScDe\eta^{10} \\ &- 79200A^2N_BRdRScDe\eta^{10} + 79200AN_BRdRScDe\eta^{10} \\ &- 26400N_BRdRScDe\eta^{10} + 11550A^2N_BR^2Sc^2\eta^9 \\ &- 23100AN_BR^2Sc^2\eta^9 + 11550N_BR^2Sc^2\eta^9 \\ &+ 15400A^2N_BRdR^2Sc^2\eta^9 - 30800AN_BRdR^2Sc^2\eta^9 \\ &+ 15400N_BRdR^2Sc^2\eta^9 - 660A^2N_BR^2Sc\eta^9 + \cdots) \end{split}$$

4. Result and discussion

(27)

A comprehensive examination on the theoretical investigation of the heat and mass transfer properties on the MHD UCM fluid flow squeezed through a channel formed by placing an impermeable moving top and stationary porous bottom plates parallel to each other is briefly discussed in this section. The repercussions of various pertinent parameters that pose a physical impact on the velocity fields, temporal distribution curves, and concentration profiles are graphically presented in Figs. 2–28. Further, Figs. 2–8 depict the velocity profile, Figs. 9–16 display for temporal distribution curve and Figs. 17–28 represents the concentration field for distinct values of the parameters considered in the problem. Moreover, the influence of these parameters on the skin friction coefficient, rates of heat, and mass transfer are numerically tabulated in Tables 1–6.

Figs. 2-8 show that lower velocities are indicated in blue and higher velocities in peach. Notably, Fig. 2 reveals that the velocity profile peaks between $0.55 \le \eta \le 0.8$ when the plates dilate $(3.5 \le R \le 5)$ and between $0.45 \le \eta \le 0.5$ when they come together $(-4.5 \le R \le -5)$. This indicates that velocity is maximized in the mid-region between the plates and decreases until it reaches the minimum at the boundaries of the plates. The repercussions of the R on the velocity distribution curve for injection and suction are presented in Figs. 2 and 3. From the figures, it is discovered that an upsurge in R elevates the velocity distribution profile as the plates approach each other for both injection (A = -0.5) and suction (A = 0.5) in the region $0 \le \eta \le 0.5$ and decreases further. In contrast, an opposite behaviour was observed as the plates dilated. Figs. 4 and 5 display graphically the sequel of injection and suction on the velocity distribution field. It is evident from the figures that the velocity of the fluid elevates with an increase in injection, whereas it decreases with an upsurge in suction for both plates moving closer and parting away. This is due to the fact that as the fluid is injected through the plate, a larger volume of fluid is introduced into the system, enhancing overall momentum and elevating flow velocity. This additional fluid contributes to shear forces, resulting in a more pronounced velocity profile. Conversely, when the fluid is sucked out, the volume of the fluid in the gap reduces, leading to a decrease in momentum that causes a vacuum effect which in turn lowers the flow velocity. In this scenario, fluid is extracted more quickly than it is replenished, resulting in a reduced velocity.

The repercussion of the magnetic parameter on the velocity profile is demonstrated in Fig. 6. It is noted that a rise in the magnetic parameter upsurges the velocity in the region $0 \le \eta \le 0.55$ and retards on the latter half for both injection and suction as the plates move towards and away from each other. This is observed due to the fact that as the magnetic parameter increases, the initial impact of the Lorentz force on fluid flow is minimal, leading to higher velocities. However, with further increases, the Lorentz force becomes dominant, raising flow resistance. Beyond a critical threshold, fluid velocity decreases, especially in later flow stages. The sequel of Deborah number on the

(31)

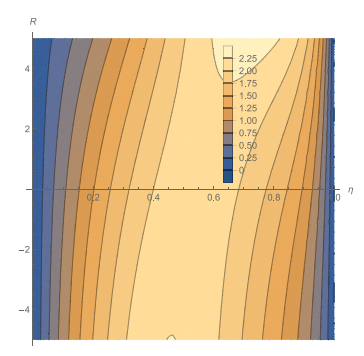


Fig. 2. Influence of R on the velocity distribution for injection case with M=0.2, De=2 and K=1.

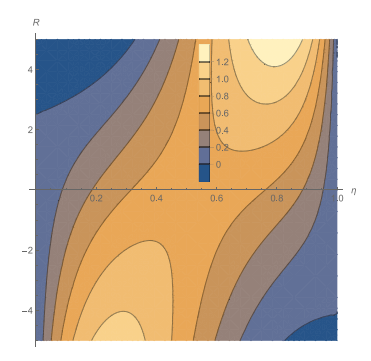


Fig. 3. Influence of R on the velocity distribution for suction case with M=0.2, De=2 and K=1.

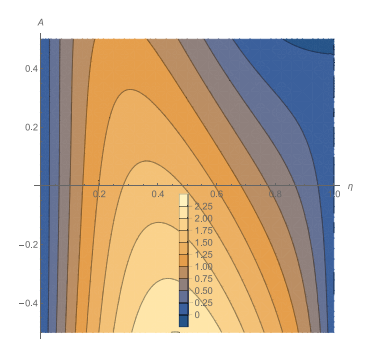


Fig. 4. Influence of A on the velocity distribution as the upper plates moves towards the lower with $M=0.2,\ De=2$ and K=1.

velocity field distribution is demonstrated in Fig. 7. It is apparent that the velocity profile retards initially and then elevates in the range $0.6 \le \eta \le 1$ with an increase in De due to elastic effects. The elastic effect initially suppresses the velocity gradient at the centre in the first half. Whereas in the second half, the elastic behaviour becomes more dominant, resulting in an increased velocity field. The sequel of the porosity parameter, K on the velocity profile is plotted graphically in Fig. 8. It is noted that the velocity profile retards with a rise in K because an increase in porosity leads to a higher resistance to flow. This leads to a decline in the overall velocity of the fluid as it moves between the plates. Additionally, the increased porosity creates more obstacles for the fluid, leading to a retardation in the velocity profile.

In Figs. 9–16, the cooler colour blue distinctly represents the cooler regions, while the warmer regions are marked by red. Furthermore, Fig. 9 reveals that the temporal profile rises more rapidly from the base (blue) to the peak value (red) when the plates approach each other, whereas this increase occurs at a slower rate during plate dilation. The sequel of R on the temporal distribution curve is presented in Fig. 9.

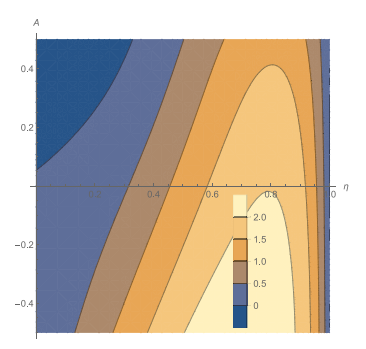


Fig. 5. Influence of A on the velocity distribution as the upper plates moves apart from the lower with M=0.2, De=2 and K=1.

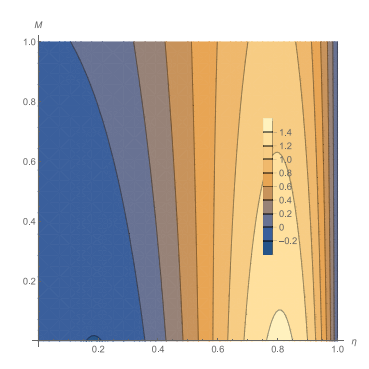


Fig. 6. Influence of M on the velocity distribution as the upper plates moves apart from the lower for suction case with De = 2 and K = 1.

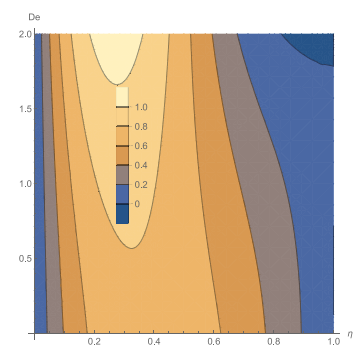


Fig. 7. Influence of De on the velocity distribution as the upper plates moves apart from the lower for suction case with M=0.2 and K=1.

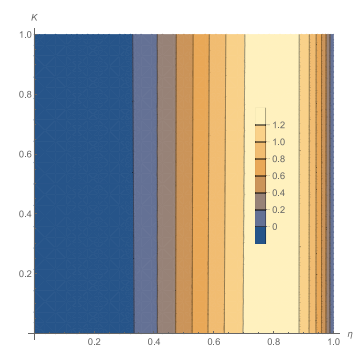


Fig. 8. Influence of K on velocity distribution as the upper plates moves apart from the lower for suction case with M=0.2 and De=2.

It is evident that the temperature profile retards with an increase in R due to the turbulence. As the plates dilate from one another, the turbulence increases, resulting in increased mixing and a more uniform distribution of temperature. As a result the temporal profile retards across the fluid layer. From Fig. 10, it can be concluded that a rise in A causes the temporal profile to decline due to the interaction of the fluid flow with the temperature gradient. When there is an increase in injection and suction, it affects the flow characteristics, leading to a reduction in the temperature profile. This phenomenon is further influenced by the changes in fluid velocity and viscosity distribution within the flow field.

Fig. 11 displays the sequel of M on the temporal profile. It has been discovered that an elevation in the magnetic parameter raises the temporal field due to the interaction of the fluid flow with the magnetic field applied externally. This interaction leads to a change in the flow characteristics, causing an increase in the temperature profile. The magnetic parameter affects the fluid flow behaviour and heat transfer, ultimately leading to the observed increment in the temperature profile. The repercussion of De on the temporal field is presented graphically in Fig. 12. It is apparent from the figures that a rise in De is associated with an elevation in the temperature field due to the enhanced visco-elastic effects. This occurs because a higher Deborah number corresponds to a higher ratio of elastic to viscous forces, causing the material to behave more like a solid. As a consequence of higher elastic force, the flow becomes more constrained, resulting in the temperature profile to elevated.

Fig. 13 shows that an upsurge in K causes a decline in the temperature profile. This can be attributed to the increased flow resistance caused by higher porosity. An elevation in the porosity parameter causes a decline in the ability of the fluid to transmit heat, leading to a depletion in the temperature. The sequel of Pr on the temporal distribution curve is presented in Fig. 14. The temporal distribution cure is found to elevate with an increase in Pr. This behaviour occurs because the Prandtl number is associated with the ratio of momentum and thermal diffusivities. A higher Pr indicates a more gradual change of momentum compared to a change in temperature, resulting in increased thermal diffusion relative to momentum diffusion. Hence, the temporal profile increases.

The sequel of Rd on the temperature field is graphically displayed in Fig. 15. An increment in the thermal radiation parameter reduces the temperature field due to the increased efficiency of heat transfer through radiation. As the radiation parameter increases, the fluid is able to dissipate heat more effectively through radiation, leading to a decrease in the temperature profile. Fig. 16 graphically shows the repercussion of the viscous dissipation represented by the Eckert number, Ec. It is observed that an upsurge in the Eckert number elevates the temporal profile due to the dissipation of energy. As the Eckert number rises, the kinetic energy of the flow is converted into thermal energy more efficiently, resulting in a higher temperature profile. This phenomenon can be attributed to the intensified heat transfer within the fluid as the Eckert number increases.

Figs. 17–28 illustrate that the colour blue represents a lower concentration, while peach signifies a higher value. From Fig. 17, it can be observed that the concentration reaches its highest point as the flow approaches the upper plate. The sequel of R on the concentration distribution profile is demonstrated in Fig. 17. An increment in the Reynolds number causes the concentration profile to reduce in the case of injection, whereas a rise in R elevates the concentration profile in the case of suction. The concentration profile is found to decline as a consequence of an elevation in R in the case of injection due to the enhanced mixing and diffusion caused by the higher flow rates. Conversely, the concentration profile elevates with a rise in R in the case of suction due to the low flow rate that reduces the mixing and diffusion. Fig. 18 demonstrates the impact of A on the concentration distribution curve. It is observed that both injection and suction increase the concentration

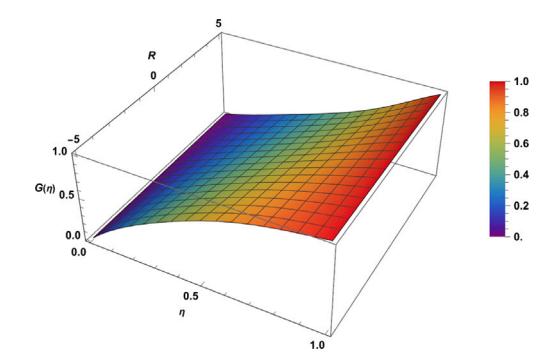


Fig. 9. Influence of R on temporal profile for suction case with M = 0.2, De = 2, K = 1 Pr = 0.5, Rd = 0.3 and Ec = 0.5.

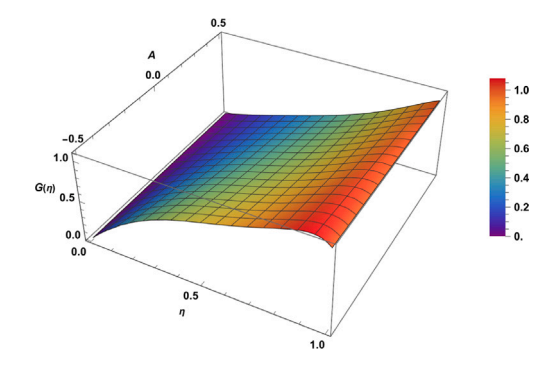


Fig. 10. Influence of *A* on temporal profile as the upper plates moves apart from the lower with M = 0.2, De = 2, K = 1 Pr = 0.5, Rd = 0.3 and Ec = 0.5.

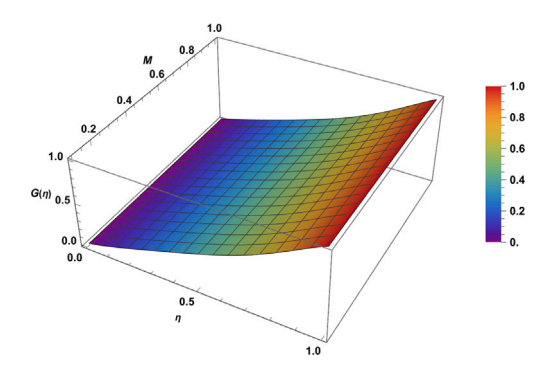


Fig. 11. Influence of M on temporal profile as the upper plates moves apart from the lower for suction case with De = 2, K = 1 Pr = 0.5, Rd = 0.3 and Ec = 0.5.

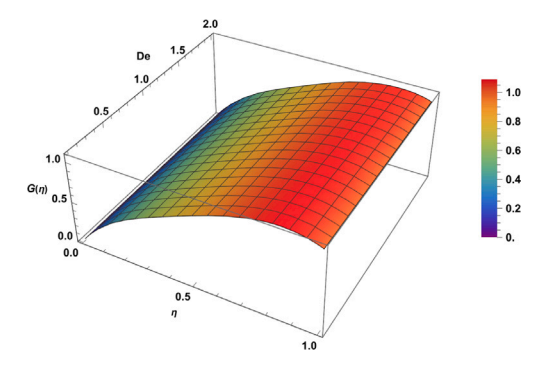


Fig. 12. Influence of De on temporal profile as the upper plates moves towards the lower for injection case with M = 0.2, K = 1 Pr = 0.5, Rd = 0.3 and Ec = 0.5.

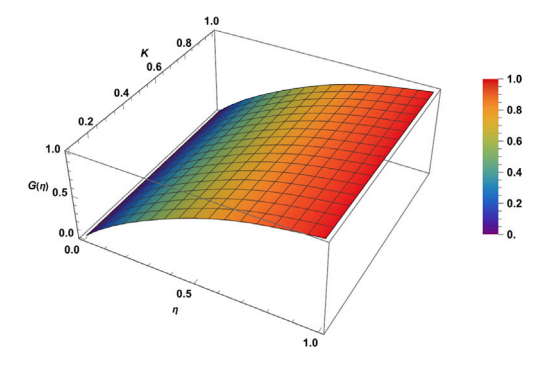


Fig. 13. Influence of K on temporal profile as the upper plates moves towards the lower for suction case with M = 0.2, De = 2 Pr = 0.5, Rd = 0.3 and Ec = 0.5.

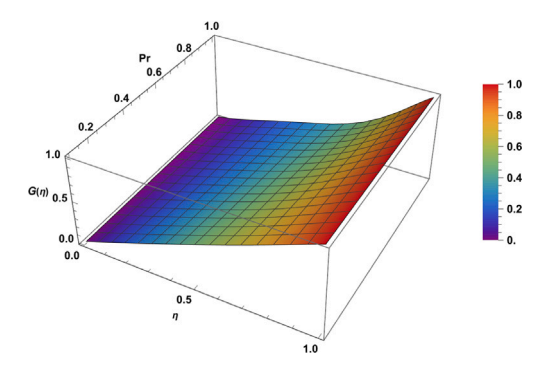


Fig. 14. Influence of Pr on temporal profile as the upper plates moves apart from the lower for suction case with M = 0.2, De = 2 K = 1, Rd = 0.3 and Ec = 0.5.

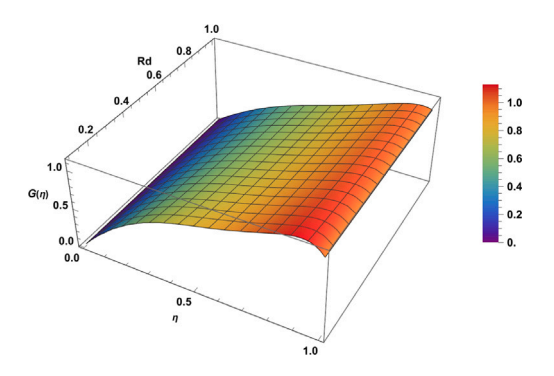


Fig. 15. Influence of Rd on temporal profile as the upper plates moves apart from the lower for injection case with M = 0.2, De = 2 K = 1, Pr = 0.5 and Ec = 0.5.

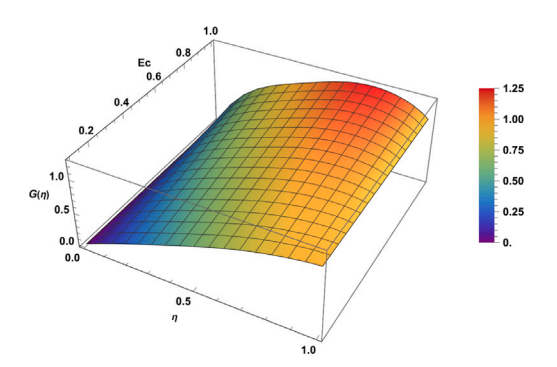


Fig. 16. Influence of Ec on temporal profile as the upper plates moves towards the lower for injection case with M=0.2, De=2 K=1, Pr=0.5 and Rd=0.3.

profile due to the combined effects of the visco-elastic behaviour of the fluid and the injection/suction flow.

The impact of M on the concentration profile is displayed in Fig. 19. An increase in the magnetic parameter decreases the concentration profile due to the interaction between the magnetic field and the fluid. This further affects the momentum and concentration boundary layer, resulting in the concentration profile to decline. From Fig. 20, it is noted that an increment in De increases the concentration distribution curve. This is observed because as the Deborah number increases, the elastic effect dominates, leading to a pronounced stretch and deformation of the fluid. Consequently, this leads to an increased concentration distribution curve.

Fig. 21 displays the sequel of K on the concentration distribution curve as the plates approach each other in the case of suction. An increment in K increases the concentration profile due to the reduced resistance to flow. The repercussion of Pr on $\phi(\eta)$ is graphically presented in Fig. 22. An increase in the Prandtl number has no significant impact on the concentration field. Due to the unique rheological properties of UCM fluids that dominate over the concentration profile making the impact of Pr relatively negligible.

The sequel of Rd on the concentration distribution curve is demonstrated in Fig. 23. The concentration profile increases with an elevation in the radiation parameter because the thermal radiation parameter directly affects the heat transfer within the fluid. An increase in Rd increases the radiative heat transfer, leading to higher temperatures that subsequently influence the concentration profile. The repercussion of Ec on the concentration profile is shown in Fig. 24. It is evident from the figure that an increase in the Eckert number decreases the concentration profile due to the enhanced convective heat transfer. As Ec increases, a greater amount of kinetic energy is converted into thermal energy, leading to a more efficient heat transfer process. This in turn reduces the concentration profile.

The repercussion of N_T on the concentration distribution curve is demonstrated in Fig. 25. It is evident that an elevation in the Nusselt number decreases the concentration profile because the thermal boundary layer is inversely proportional to the Nusselt number, that is, as the Nusselt number elevates, the thermal boundary layer becomes thinner. This occurs because N_T characterizes heat transfer efficiency, as a result, the concentration profile retards. Fig. 26 demonstrates the repercussion of N_B on the concentration distribution field for the case of injection as the plates move apart. It is evident that with an increase in the Brownian motion parameter, the concentration distribution field increases. This occurs due to the fact that as the Brownian motion parameter increases, the random motion of the particles becomes more significant, enhancing the mass diffusion. As a result of enhanced mass diffusion, the concentration profile increases.

The influence of Sc on the concentration field is depicted in Fig. 27. From the figures, it is noticed that a rise in the Schmidt number elevates the concentration distribution curve. This phenomenon occurs due to the dominance of momentum diffusivity over mass diffusivity. Further, Fig. 28 shows the repercussion of Kr on the concentration distribution curve for plates dilating from one another in the case of suction. It is apparent that an elevation in Kr causes the concentration profile to retard for both injection and suction. This behaviour is observed due to the fact that a rise in the chemical reaction parameter elevates the reaction rate, further leading to a significant depletion in the concentration of the fluid, resulting in the reduction of the concentration profile.

Tables 1–4 display the repercussions of the pertinent physical parameters on the numerical values corresponding to the skin friction coefficient, and rates of heat and mass transfer. It can be concluded from the tables that the skin friction coefficient elevates with an upsurge in Reynolds number at the upper plate whereas retards at the lower. A similar trend is evident in the rate of heat and mass transfer with an elevation in R. Moreover, it is also observed that an elevation in Rd leads to a retardation in the magnitude rate of heat

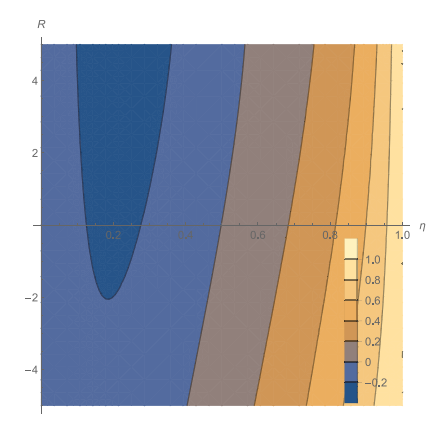


Fig. 17. Influence of R on the concentration field for injection case with M=0.2, $De=2\ K=1$, Pr=0.5, Rd=0.3, Ec=0.5, $N_T=0.5$, $N_B=0.3$, Sc=0.5 and Kr=0.5.

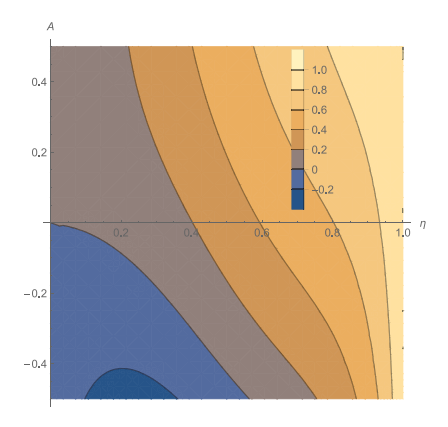


Fig. 18. Influence of *A* on the concentration field as the upper plates moves apart from the lower with M=0.2, De=2 K=1, Pr=0.5, Rd=0.3, Ec=0.5, $N_T=0.5$, $N_B=0.3$, Sc=0.5 and Kr=0.5.

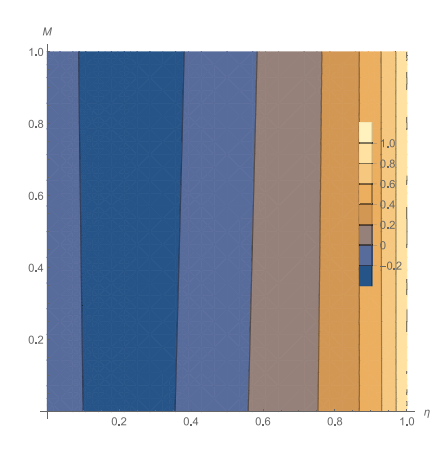


Fig. 19. Influence of M on the concentration field as the upper plates moves apart from the lower for injection case with De=2, K=1, Pr=0.5, Rd=0.3, Ec=0.5, $N_T=0.5$, $N_B=0.3$, Sc=0.5 and Kr=0.5.

transfer except for the plates moving apart in the case of suction at the lower plate. Whereas an opposite behaviour is evident from the tables as the Eckert number increases. Similarly, an increase in the Nusselt number reduces the magnitude of the rate of mass transfer except for plates dilating in the case of injection. Furthermore, Tables 5 and 6 present the comparison of the skin friction value with the literature and the numerical values obtained by the Runge–Kutta method of order four, respectively. It is apparent from the two tables that the solutions

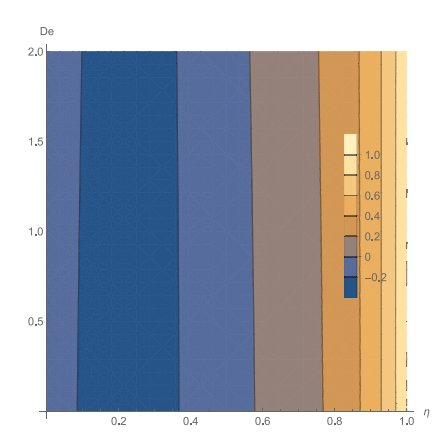


Fig. 20. Influence of De on the concentration field as the upper plates moves apart from the lower for suction case with M=0.2, K=1, Pr=0.5, Rd=0.3, Ec=0.5, $N_T=0.5$, $N_B=0.3$, Sc=0.5 and Kr=0.5.

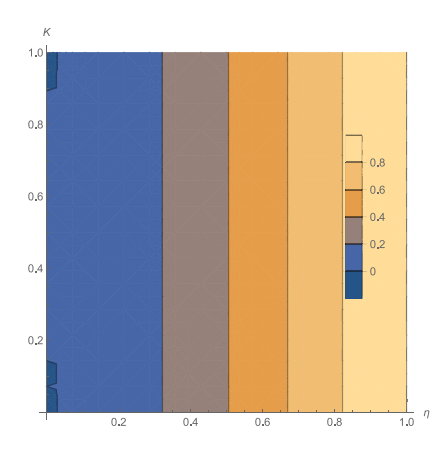


Fig. 21. Influence of K on the concentration field as the upper plates moves towards the lower for injection case with M=0.2, De=2, Pr=0.5, Rd=0.3, Ec=0.5, $N_T=0.5$, $N_B=0.3$, Sc=0.5 and Kr=0.5.

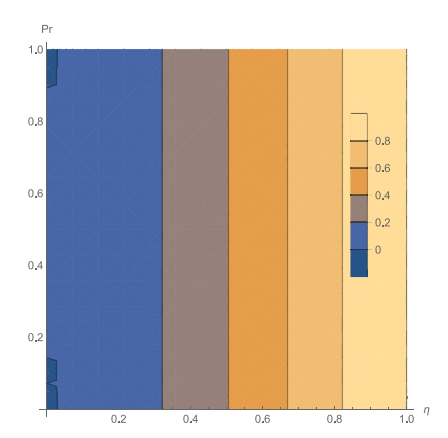


Fig. 22. Impact of Pr on concentration distribution for A=0.5 and R=-5. Influence of Pr on the concentration field as the upper plates moves towards the lower for suction case with M=0.2, De=2, K=1, Rd=0.3, Ec=0.5, $N_T=0.5$, $N_B=0.3$, Sc=0.5 and Kr=0.5.

obtained by the two methods are in good agreement with one another and the literature.

5. Conclusion

The current research work demonstrates the impact of various pertinent physical parameters on the heat and mass transfer characteristics

Table 1 Coefficient of skin friction, rate of heat and mass transfer for different values of R and A.

R	\boldsymbol{A}	F''(0)	F"(1)	$\theta'(0)$	$\theta'(1)$	$\phi'(0)$	$\phi'(1)$
-5	-0.5	-10.2135	13.3945	-3.39872	1.16213	2.28198	-2.63809
	-0.1	-8.81915	6.97686	-2.91015	0.23959	1.48884	-1.55941
	0.1	-8.6324	4.12181	-2.69953	-0.0695541	1.00252	-1.20091
	0.5	-8.84247	-0.464999	-2.31582	-0.378614	0.106357	-0.807805
-1	-0.5	-8.73721	18.9333	-3.16715	1.61047	2.63639	-4.83774
	-0.1	-5.98673	12.3999	-2.2506	0.443197	1.08772	-3.09276
	0.1	-5.05064	9.19655	-1.9104	-0.0144695	0.4768	-2.408
	0.5	-3.47791	3.44549	-1.42366	-0.625958	-0.43698	-1.47449
1	-0.5	-7.60498	23.265	-3.02719	1.92714	2.79381	-5.82357
	-0.1	-4.36408	17.083	-1.94333	0.61318	0.871671	-3.69629
	0.1	-3.2432	13.7813	-1.56763	0.0520196	0.218018	-2.82364
	0.5	-1.34668	7.17294	-1.07242	-0.785562	-0.628495	-1.57311
5	-0.5	-4.3718	35.7669	-2.71813	2.76522	3.04267	-7.55427
	-0.1	-0.797399	31.0869	-1.38987	1.11012	0.380328	-4.56864
	0.1	0.220874	27.6152	-0.997377	0.280522	-0.317215	-3.27589
	0.5	1.65967	18.399	-0.561919	-1.16793	-0.867557	-1.30687

Table 2 Coefficient of skin friction, rate of heat and mass transfer for different values of M, De and K

K	De	M	F''(0)	F"(1)	$\theta'(0)$	$\theta'(1)$	$\phi'(0)$	$\phi'(1)$
			A = -0.5					
			R = -5					
0.3	0.2	0.1	-10.0366	7.49628	-3.43671	1.18155	2.56215	-2.40402
		0.3	-9.92618	7.35401	-3.44773	1.16523	2.56614	-2.39799
	0.6	0.1	-10.0725	7.84361	-3.44266	1.15908	2.49228	-2.45947
		0.3	-9.97115	7.59533	-3.46606	1.13269	2.50678	-2.44273
0.9	0.2	0.1	-10.1013	7.56834	-3.43223	1.19044	2.56304	-2.40461
		0.3	-9.98987	7.42785	-3.44282	1.17376	2.56703	-2.39859
	0.6	0.1	-10.1306	7.94779	-3.43611	1.16992	2.4933	-2.46027
		0.3	-10.0276	7.70166	-3.45891	1.14314	2.50781	-2.44355
			R = 5					
0.3	0.2	0.1	-7.01167	13.8871	-3.21685	2.05077	3.33834	-7.34699
		0.3	-7.26037	13.9743	-3.224	2.03308	3.34479	-7.34267
	0.6	0.1	-6.53911	16.3299	-3.11915	2.19268	3.26799	-7.40096
		0.3	-6.79764	16.2962	-3.13352	2.16381	3.28532	-7.38638
0.9	0.2	0.1	-7.16477	13.9813	-3.21869	2.04358	3.33896	-7.34746
		0.3	-7.41001	14.0677	-3.2261	2.02622	3.3454	-7.34313
	0.6	0.1	-6.69848	16.481	-3.11911	2.18773	3.26848	-7.40123
		0.3	-6.95295	16.4464	-3.13357	2.15919	3.28578	-7.38663
			A = 0.5					
			R = -5					
0.3	0.2	0.1	-5.38797	1.89035	-2.183	-1.38379	0.16006	-0.83145
		0.3	-5.41934	1.8313	-2.18943	-1.39024	0.160574	-0.82885
	0.6	0.1	-5.92283	1.69781	-2.21196	-1.3344	0.14576	-0.82728
		0.3	-6.03515	1.59259	-2.22458	-1.34683	0.149329	-0.82130
0.9	0.2	0.1	-5.38369	1.9228	-2.18061	-1.38605	0.160757	-0.83210
		0.3	-5.41385	1.86529	-2.18699	-1.39244	0.161274	-0.82951
	0.6	0.1	-5.91033	1.75564	-2.20931	-1.37382	0.146495	-0.82802
		0.3	-6.02041	1.6522	-2.22184	-1.38158	0.150079	-0.82205
			R = 5					
0.3	0.2	0.1	-1.61786	6.72839	-0.686823	-1.38379	-0.807968	-1.33822
		0.3	-1.69926	6.68149	-0.689014	-1.39024	-0.80535	-1.33766
	0.6	0.1	-1.17929	8.44163	-0.659995	-1.3344	-0.822752	-1.33337
		0.3	-1.29128	8.28649	-0.662703	-1.34683	-0.816767	-1.32981
0.9	0.2	0.1	-1.66526	6.72427	-0.688051	-1.38605	-0.807358	-1.33882
		0.3	-1.74498	6.67832	-0.69027	-1.39244	-0.804748	-1.33826
	0.6	0.1	-1.23996	8.45232	-0.661014	-1.33635	-0.82218	-1.33389
		0.3	-1.350028	8.29888	-0.66373	-1.3487	-0.816215	-1.33032

of the UCM fluid flow. The study involves the flow of UCM fluid through a channel comprising an impermeable moving upper plate and a stationary porous lower plate, taking into account the injection and suction of fluid through the lower porous plate. Further, the influences of thermal radiation, viscous dissipation, and an external magnetic field on the flow are considered. Due to its extensive applications across numerous industrial and engineering arena, particularly in liquid purification, lubrication, and bearing systems, the theoretical analysis on these kind of fluids are essential to predict the outcome. Moreover, the study on the UCM fluid being limited to the flow and heat transfer with

the impacts of thermal radiation and magnetic fields only makes it difficult to accurately predict the practical model. Thus, this study strives to bridge the gap between the theoretical and practical study by inculcating the impacts of viscous dissipation and chemical reaction in the flow characteristics. To analyse the situation encountered, the repercussions of the pertinent physical parameters are analysed graphically with the help of velocity, temperature, and concentration distribution curves and tabulating the numerical values corresponding to the skin friction coefficient, and rates of heat and mass transfer. In summary, the authors have arrived at the following conclusion in this study:

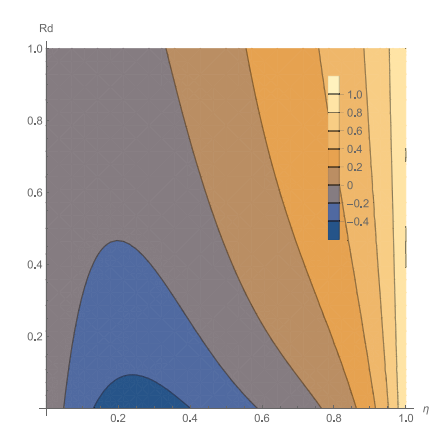


Fig. 23. Influence of Rd on the concentration field as the upper plates moves apart from the lower for injection case with M=0.2, De=2, K=1, Pr=0.5, Ec=0.5, $N_T=0.5$, $N_B=0.3$, Sc=0.5 and Kr=0.5.

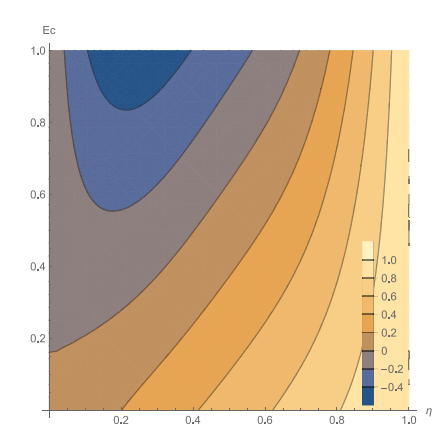


Fig. 24. Influence of Ec on the concentration field as the upper plates moves towards the lower for injection case with M=0.2, De=2, K=1, Pr=0.5, Rd=0.3, $N_T=0.5$, $N_B=0.3$, Sc=0.5 and Kr=0.5.

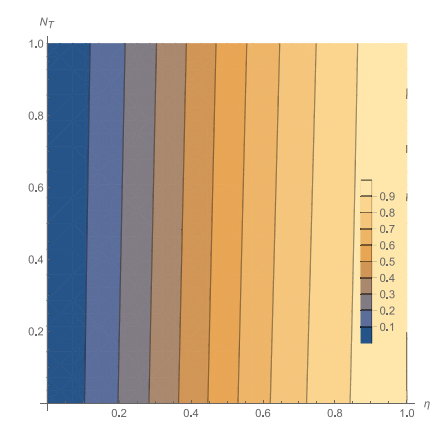


Fig. 25. Influence of N_T on the concentration field as the upper plates moves towards the lower for injection case with M=0.2, De=2, K=1, Pr=0.5, Rd=0.3, Ec=0.5, $N_B=0.3$, Sc=0.5 and Kr=0.5.

- An increment in the radiation parameter reduces the temporal distribution, whereas elevates the concentration profile.
- An elevation in the Eckert number causes the temporal distribution field to elevate, whereas the concentration profile to retard.
- Prandtl number has no significant impact on the concentration profile.

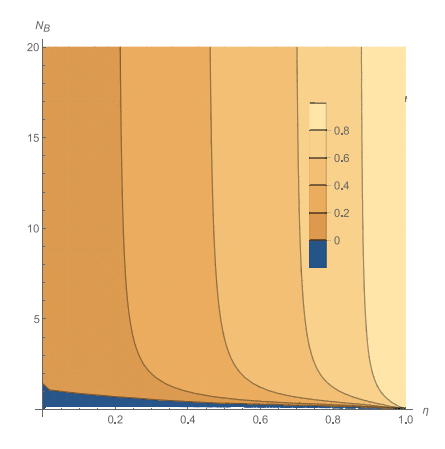


Fig. 26. Influence of N_B on the concentration field as the upper plates moves apart from the lower for injection case with M=0.2, De=2, K=1, Pr=0.5, Rd=0.3, Ec=0.5, $N_T=0.5$, Sc=0.5 and Kr=0.5.

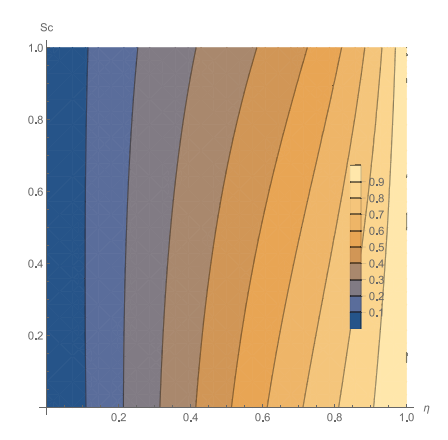


Fig. 27. Influence of Sc on the concentration field as the upper plates moves apart from the lower for injection case with M=0.2, De=2, K=1, Pr=0.5, Rd=0.3, Ec=0.5, $N_T=0.5$, $N_B=0.3$ and Kr=0.5.

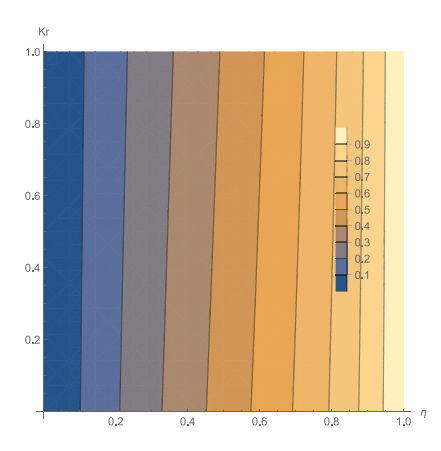


Fig. 28. Influence of Kr on the concentration field as the upper plates moves apart from the lower for suction case with M=0.2, De=2, K=1, Pr=0.5, Rd=0.3, Ec=0.5, $N_T=0.5$, $N_B=0.3$ and Sc=0.5.

- An upsurge in the Nusselt number and chemical reaction parameter results in the concentration distribution curve to decline.
- Brownian motion constant and Schmidt number increases the concentration profile.

Table 3 Rate of heat and mass transfer for different values of Pr, Rd and Ec.

Pr	Rd	Ec	$\theta'(0)$	$\theta'(1)$	$\phi'(0)$	$\phi'(1)$
			A = -0.5			
			R = -5			
0.3	0.2	0.1	-1.31019	-0.458196	-0.516432	-1.11154
		0.3	-1.97931	0.0409636	0.398123	-1.62879
	0.6	0.1	-1.22441	-0.602059	-0.62022	-0.97134
		0.3	-1.70465	-0.235551	0.0393335	-1.36446
0.9	0.2	0.1	-1.77966	0.237388	-0.0442184	-1.38686
		0.3	-3.5534	1.39543	2.23968	-2.1002
	0.6	0.1	-1.59198	-0.0217695	-0.204983	-1.4088
		0.3	-2.90778	0.884281	1.546	-2.17299
			R = 5			
0.3	0.2	0.1	-1.27603	-0.768465	-0.513776	-2.0187
		0.3	-1.67886	0.314174	0.522317	-3.76067
	0.6	0.1	-1.19059	-0.837495	-0.690728	-1.97754
		0.3	-1.46455	-0.0947196	0.022397	-3.17423
0.9	0.2	0.1	-1.94384	-0.285512	0.804216	-2.26726
		0.3	-3.46213	3.61081	4.37227	-8.33158
	0.6	0.1	-1.62639	-0.50458	0.191868	-2.16308
		0.3	-2.59246	2.01945	2.55892	-6.16835
			A = 0.5			
			R = -5			
0.3	0.2	0.1	-1.53923	-0.552361	-1.02251	-0.709733
		0.3	-1.69421	-0.542407	-0.831512	-0.72769
	0.6	0.1	-1.37079	-0.664875	-1.32221	-0.63232
		0.3	-1.47913	-0.656172	-1.18916	-0.647985
0.9	0.2	0.1	-2.83161	-0.183376	1.32766	-0.484165
		0.3	-3.31463	-0.198044	1.9397	-0.450889
	0.6	0.1	-2.22735	-0.26871	0.212779	-0.7453
		0.3	-2.56201	-0.265763	0.631261	-0.74914
			R = 5			
0.3	0.2	0.1	-0.69719	-1.45181	-0.513776	-1.30351
		0.3	-0.695188	-1.26309	0.522317	-1.53027
	0.6	0.1	-0.778779	-1.29945	-0.690728	-1.6781
		0.3	-0.778258	-1.16854	0.022397	-1.83463
0.9	0.2	0.1	-0.358241	-2.9358	0.804216	1.90632
		0.3	-0.324022	-2.31082	4.37227	1.13892
	0.6	0.1	-0.460046	-2.1734	0.191868	0.333191
		0.3	-0.445195	-1.75266	2.55892	-0.179577

Future scope

In totality, the current work is limited to the theoretical study on the sequel of viscous dissipation and thermal radiation on the characteristics of heat and mass transfer in the MHD UCM fluid flow through a porous channel with a moving upper plate. However, a further study on the ion slip, temperature jump, activation energy, and nanoparticle affect on the flow, heat and mass transfer can be analysed theoretically. Moreover, this theoretical approach can be experimentally investigated for a better understanding of industrial and engineering applications.

CRediT authorship contribution statement

Pareekshith G. Bhat: Writing – original draft, Visualization, Software, Formal analysis, Conceptualization. Ali J. Chamkha: Writing – review & editing, Validation, Investigation, Formal analysis. Nityanand P. Pai: Writing – review & editing, Supervision, Resources, Methodology. Sampath Kumar V.S.: Validation, Supervision, Project administration, Investigation, Data curation.

Declaration of competing interest

The authors declare the following financial interests/personal relationships which may be considered as potential competing interests: Sampath Kumar V. S. reports a relationship with Manipal Academy of Higher Education that includes: employment. Authors declare that they have no known competing financial interests or personal relationships that could have appeared to influence the work reported in this paper.

Table 4
Rate of mass transfer for different values of N_T , N_D , S_C and K_L

N_B	Sc	Kr	$N_T = 0.5$		$N_T = 1$	
			$\phi'(0)$	φ'(1)	$\phi'(0)$	φ'(1)
			A = -0.5			
			R = -5			
10	0.2	0.1	-0.868575	-0.842621	-0.759888	-0.93173
		0.3	-0.862774	-0.854125	-0.754356	-0.94295
	0.6	0.1	-0.814813	-0.476601	-0.721903	-0.53291
		0.3	-0.800868	-0.503088	-0.708765	-0.55853
20	0.2	0.1	-0.922918	-0.798062	-0.868575	-0.84262
		0.3	-0.916983	-0.80971	-0.862774	-0.85412
	0.6	0.1	-0.861268	-0.448444	-0.814813	-0.47660
		0.3	-0.84692	-0.475362	-0.800868	-0.50308
			R = 5			
10	0.2	0.1	-0.945079	-1.41914	-0.830134	-1.57498
		0.3	-0.937967	-1.43388	-0.823235	-1.58953
	0.6	0.1	-1.02302	-2.18071	-0.894522	-2.35722
		0.3	-0.997988	-2.23513	-0.870132	-2.41106
20	0.2	0.1	-1.00255	-1.34122	-0.945079	-1.41914
		0.3	-0.995333	-1.35606	-0.937967	-1.43388
	0.6	0.1	-1.08727	-2.09245	-1.02302	-2.18071
		0.3	-1.06192	-2.14717	-0.997988	-2.23513
			A = 0.5			
			R = -5			
10	0.2	0.1	-1.32164	-0.646435	-1.26299	-0.67246
		0.3	-1.31299	-0.658803	-1.25447	-0.68469
	0.6	0.1	-2.22131	-0.236697	-2.15635	-0.24792
		0.3	-2.1813	-0.263782	-2.11675	-0.27458
20	0.2	0.1	-1.35097	-0.633419	-1.32164	-0.64643
		0.3	-1.34225	-0.645858	-1.31299	-0.65880
	0.6	0.1	-2.25379	-0.231085	-2.22131	-0.23669
		0.3	-2.21358	-0.258381	-2.1813	-0.26378
			R = 5			
10	0.2	0.1	-0.753156	-1.42735	-0.769037	-1.39898
		0.3	-0.748276	-1.44099	-0.764076	-1.41271
	0.6	0.1	-0.422001	-2.75301	-0.43385	-2.71562
		0.3	-0.416677	-2.78995	-0.428282	-2.75282
20	0.2	0.1	-0.745215	-1.44153	-0.753156	-1.42735
		0.3	-0.740377	-1.45512	-0.748276	-1.44099
	0.6	0.1	-0.416076	-2.7717	-0.422001	-2.75301
		0.3	-0.410875	-2.80851	-0.416677	-2.78995

Acknowledgements

The authors are thankful to the Manipal Academy of Higher Education, Manipal; Kuwait College of Science and Technology, Kuwait and NMAM Institute of Technology, Nitte for their support.

Appendix. Dimensionless physical parameters

Physical parameter	Notation	Formula
Reynolds number	R	$R = \frac{hV_h}{v}$
Magnetic parameter	M	$M = rac{\sigma B_0^2 h}{ ho V_h}$
Deborah number	De	$De = \frac{\lambda V_h^2}{V}$
Porosity parameter	K	$K = \frac{h^2 \omega}{k}$
Prandtl number	Pr	$K = \frac{h^2 \omega}{k}$ $Pr = \frac{C_{P} \mu}{k_0}$
Eckert number	Ec	$Ec = \frac{V_h}{C_P(T_2 - T_1)}$
Radiation parameter	Rd	$Rd = \frac{4\sigma^* T_1^3}{k_0 k^*}$
Nusselt number	N_T	$N_T = \frac{D_T^{\circ}(T_2 - T_1)}{T_1 v}$
Schmidt number	Sc	$Sc = \frac{v}{D_B}$
Brownian motion constant	N_B	$N_B = \frac{D_B(C_2 - C_1)}{v}$ $Kr = \frac{k_1 h^2}{v}$
Chemical reaction parameter	Kr	$Kr = \frac{k_1 h^2}{v}$

Table 5 Coefficient of skin friction, rate of heat and mass transfer for different values of R and A for M = 0.2, De = 0.2 and K = 0.1.

R	\boldsymbol{A}	F''(0)		F"(1)	
		HPM	RK - 4	НРМ	RK - 4
-1	-0.5	-9.22227	-9.22217	8.73114	8.73144
	-0.3	-8.09895	-8.09883	7.44782	7.44811
	0	-6.38743	-6.38727	5.57464	5.57501
	0.3	-4.61803	-4.61796	3.77723	3.77784
	0.5	-3.38787	-3.38823	2.63037	2.63117
0	-0.5	-8.97085	-8.97074	9.25371	9.25508
	-0.3	-7.73429	-7.73419	8.01968	8.02082
	0	-5.92682	-5.92675	6.15398	6.15476
	0.3	-4.15148	-4.15143	4.28453	4.28499
	0.5	-2.97429	-2.97425	3.04395	3.04421
1	-0.5	-8.6836	-8.68289	9.888	9.89545
	-0.3	-7.34138	-7.34085	8.71846	8.72614
	0	-5.4648	-5.46448	6.86654	6.87414
	0.3	-3.7145	-3.71442	4.91143	4.91835
	0.5	-2.60469	-2.60481	3.55624	3.56225
		$\theta'(0)$		$\theta'(1)$	
-1	-0.5	-3.4138	-3.41351	1.35161	1.35185
	-0.3	-2.8731	-2.87288	0.779857	0.780053
	0	-2.1903	-2.19036	0.090842	0.0910873
	0.3	-1.67142	-1.67194	-0.401069	-0.40077
	0.5	-1.42349	-1.42421	-0.623229	-0.62297
0	-0.5	-3.39189	-3.39159	1.42992	1.43033
	-0.3	-2.79413	-2.7939	0.827626	0.827944
	0	-2.06131	-2.06117	0.0817371	0.0819237
	0.3	-1.52099	-1.52093	-0.470936	-0.47085
	0.5	-1.26648	-1.26645	-0.730749	-0.73071
1	-0.5	-3.36517	-3.3638	1.52242	1.52641
	-0.3	-2.71329	-2.71242	0.888539	0.892736
	0	-1.93725	-1.93691	0.0799909	0.0838382
	0.3	-1.38145	-1.38141	-0.542384	-0.53951
	0.5	-1.12313	-1.12318	-0.846422	-0.84446
		φ'(0)		φ'(1)	
-1	-0.5	2.89758	2.90799	-4.57477	-4.60404
	-0.3	2.03507	2.04206	-3.6767	-3.69936
	0	0.910218	0.917883	-2.5919	-2.60549
	0.3	0.022154	0.0314114	-1.81297	-1.8193
	0.5	-0.417756	0.409609	-1.45704	-1.46018
0	-0.5	2.97904	2.97755	-5.07869	-5.08359
	-0.3	1.99486	1.99357	-4.08786	-4.09178
	0	0.78823	0.787347	-2.86102	-2.86342
	0.3	-0.101521	-0.101965	-1.95211	-1.95322
	0.5	-0.520709	-0.520879	-1.52487	-1.52534
1	-0.5	3.05837	3.03885	-5.56614	-5.60934
	-0.3	1.95194	1.93613	-4.47887	-4.52085
	0	0.666543	0.658009	-3.10437	-3.13887
	0.3	0.217184	0.220696	-2.05979	-2.08297
	0.5	-0.607877	-0.609646	-1.55741	-1.57217

Table 6 Comparison of the coefficient of skin friction for De = K = M = 0.

R	\boldsymbol{A}	F''(0)				
		Present study		Terrill et al.	[5]	
		HPM	RK - 4	Series	Numerical	
0.23842	-0.70503	10.1991	10.1991	10.19906	10.19902	
0.81110	-0.93519	11.6917	11.6917	11.6918	11.6917	
-0.77394	-0.24575	7.77871	7.77871	7.7786	7.7782	
0.42766	0.52767	2.68712	2.68711	2.68704	2.68709	
0.84194	0.48575	2.78615	2.78612	2.7857	2.7861	
0.23842	-0.70503	-10.3218	-10.3218	-10.3217	-10.3218	
0.81110	-0.93519	-11.8032	-11.8032	-11.8027	-11.8032	
-0.77394	-0.24575	-7.08987	-7.08991	-7.091	-7.089	
0.42766	0.52767	-2.99929	-2.99929	-2.99918	-2.99927	
0.84194	0.48575	-3.44565	-3.44559	-3.4449	-3.4456	

Data availability

No data was used for the research described in the article.

References

- [1] Archimedes, On floating bodies, book i, in: T.L. Heath (Ed.), The Works of Archimedes: Edited in Modern Notation with Introductory Chapters, Cambridge University Press, Cambridge, 2009, pp. 253–262, http://dx.doi.org/10.1017/ CBO9780511695124.019.
- [2] E.A. Hamza, Suction and injection effects on a similar flow between parallel plates, J. Phys. D: Appl. Phys. 32 (6) (1999) 656–663, http://dx.doi.org/10. 1088/0022-3727/32/6/010.
- [3] Q. Ghori, M. Ahmed, A. Siddiqui, Application of homotopy perturbation method to squeezing flow of a Newtonian fluid, Int. J. Nonlinear Sci. Numer. Simul. 8 (2) (2007) 179–184, http://dx.doi.org/10.1515/JJNSNS.2007.8.2.179.
- [4] U. Khan, N. Ahmed, S.I. Khan, S. Bano, S.T. Mohyud-din, Unsteady squeezing flow of a casson fluid between parallel plates, World J. Model. Simul. 10 (4) (2014) 308–319.
- [5] R.M. Terrill, G.M. Shrestha, Laminar flow through parallel and uniformly porous walls of different permeability, J. Appl. Math. Phys. (ZAMP) 16 (1965) 470–482, http://dx.doi.org/10.1007/BF01593923.
- [6] P. Jalili, A.A. Azar, B. Jalili, D.D. Ganji, A novel analytical investigation of a swirling fluid flow and a rotating disk in the presence of uniform suction, Arab. J. Sci. Eng. 49 (8) (2024) 10453–10469, http://dx.doi.org/10.1007/s13369-023-08391-7.
- [7] W.F. Hughes, R.A. Elco, Magnetohydrodynamic lubrication flow between parallel rotating disks, J. Fluid Mech. 13 (1) (1962) 21–32, http://dx.doi.org/10.1017/ S0022112062000464.
- [8] D.C. Kuzma, E.R. Maki, R.J. Donnelly, The magnetohydrodynamic squeeze film, J. Fluid Mech. 19 (3) (1964) 395–400, http://dx.doi.org/10.1017/ S0022112064000805.
- [9] D.C. Kuzma, Fluid inertia effects in squeeze films, Appl. Sci. Res. 18 (1968) 15–20, http://dx.doi.org/10.1007/BF00382330.
- [10] S.G. Bejawada, M.M. Nandeppanavar, Effect of thermal radiation on magnetohydrodynamics heat transfer micropolar fluid flow over a vertical moving porous plate, Exp. Comput. Multiph. Flow 5 (2) (2023) 149–158, http://dx.doi.org/10. 1007/s42757-021-0131-5.
- [11] K. Raghunath, M. Obulesu, K. Venkateswara Raju, Radiation absorption on MHD free conduction flow through porous medium over an unbounded vertical plate with heat source, Int. J. Ambient Energy 44 (1) (2023) 1712–1720, http://dx.doi.org/10.1080/01430750.2023.2181869.
- [12] D. Ali, H. Ullah, A.M. Alqahtani, M. Fiza, A.S. Omer, I. Khan, A.U. Jan, Numerical treatment of squeezed fluid flow under the magnetic influence amid parallel disks, Int. J. Thermofluids (2024) 100723, http://dx.doi.org/10.1016/j.ijft.2024. 100723
- [13] M. Mahboobtosi, A.M. Ganji, P. Jalili, B. Jalili, I. Ahmad, A.S. Hendy, M.R. Ali, D. Ganji, Investigate the influence of various parameters on MHD flow characteristics in a porous medium, Case Stud. Therm. Eng. 59 (2024) 104428, http://dx.doi.org/10.1016/j.csite.2024.104428.
- [14] M.M. Syam, M.I. Syam, Computational study of magnetohydrodynamic squeeze flow between infinite parallel disks, Int. J. Thermofluids 24 (2024) 100847, http://dx.doi.org/10.1016/j.ijft.2024.100847.
- [15] Y.J. Kim, Unsteady MHD convective heat transfer past a semi-infinite vertical porous moving plate with variable suction, Internat. J. Engrg. Sci. 38 (8) (2000) 833–845, http://dx.doi.org/10.1016/S0020-7225(99)00063-4.
- [16] R. Cortell, Flow and heat transfer in a moving fluid over a moving flat surface, Theor. Comput. Fluid Dyn. 21 (2007) 435–446, http://dx.doi.org/10. 1007/s00162-007-0056-z.
- [17] M.G. Reddy, M.V.V.N.L. Sudharani, M.M. Praveena, K.G. Kumar, Effect of thermal conductivity on Blasius–Rayleigh–Stokes flow and heat transfer over a moving plate by considering magnetic dipole moment, Eur. Phys. J. Plus 137 (1) (2021) 29, http://dx.doi.org/10.1140/epjp/s13360-021-02259-1.
- [18] A. Shateri, M.M. Moghaddam, B. Jalili, Y. Khan, P. Jalili, D.D. Ganji, Heat transfer analysis of unsteady nanofluid flow between moving parallel plates with magnetic field: Analytical approach, J. Central South Univ. 30 (7) (2023) 2313–2323, http://dx.doi.org/10.1007/s11771-023-5388-3.
- [19] A.A. Azar, P. Jalili, Z.P. Moziraji, B. Jalili, D.D. Ganji, Analytical solution for MHD nanofluid flow over a porous wedge with melting heat transfer, Heliyon 10 (15) (2024) http://dx.doi.org/10.1016/j.heliyon.2024.e34888.
- [20] V.M. Behera, S.K. Rathore, Heat transfer augmentation by plate motion in a wall jet flow over a heated plate: A conjugate heat transfer technique, Numer. Heat Transf. Part A: Appl. 85 (14) (2024) 2280–2297, http://dx.doi.org/10.1080/ 10407782.2023.2220906.
- [21] B. Jalili, A.A. Azar, P. Jalili, D. Liu, M.A. Abdelmohimen, D.D. Ganji, Investigation of the unsteady MHD fluid flow and heat transfer through the porous medium asymmetric wavy channel, Case Stud. Therm. Eng. 61 (2024) 104859, http://dx.doi.org/10.1016/j.csite.2024.104859.
- [22] B. Jalili, A.A. Azar, D. Liu, P. Jalili, C. Kang, D.D. Ganji, Analytical formulation of the steady-state planar Taylor–Couette flow constitutive equations with entropy considerations, Phys. Fluids 36 (11) (2024) http://dx.doi.org/10.1063/ 5.0239765.

- [23] B. Jalili, P.M. Zar, D. Liu, C.-H. Ji, P. Jalili, M.A. Abdelmohimen, D.D. Ganji, Thermal study of MHD hybrid nano fluids confined between two parallel sheets: shape factors analysis, Case Stud. Therm. Eng. 63 (2024) 105229, http://dx.doi. org/10.1016/j.csite.2024.105229.
- [24] A. Mirzaei, B. Jalili, P. Jalili, D.D. Ganji, Free convection in a square wavy porous cavity with partly magnetic field: a numerical investigation, Sci. Rep. 14 (1) (2024) 14152, http://dx.doi.org/10.1038/s41598-024-64850-7.
- [25] A.J. Chamkha, Effects of heat absorption and thermal radiation on heat transfer in a fluid-particle flow past a surface in the presence of a gravity field, Int. J. Therm. Sci. 39 (5) (2000) 605–615, http://dx.doi.org/10.1016/S1290-0729(00) 00209-X.
- [26] K. Das, Impact of thermal radiation on MHD slip flow over a flat plate with variable fluid properties, Heat Mass Transf. 48 (5) (2012) 767–778, http://dx. doi.org/10.1007/s00231-011-0924-3.
- [27] A. Raptis, C. Perdikis, H. Takhar, Effect of thermal radiation on MHD flow, Appl. Math. Comput. 153 (3) (2004) 645–649, http://dx.doi.org/10.1016/S0096-3003(03)00657-X.
- [28] U. Farooq, A. Jan, M. Hussain, Impact of thermal radiations, heat generation/absorption and porosity on MHD nanofluid flow towards an inclined stretching surface: Non-similar analysis, Z. Für Angew. Math. Und Mech. (ZAMM-J. Appl. Math. Mechanics) 104 (3) (2024) e202300306, http://dx.doi.org/10.1002/zamm. 202300306.
- [29] K.G. Kumar, N. Vidyarani, R. Padmavathi, H. Lokesh, D. Prakasha, D. Abduvalieva, M.I. Khan, et al., Analyzing the influence of magnetic dipole on non-Newtonian fluid flow over a sheet with non-uniform radiation, Partial. Differ. Equations Appl. Math. 11 (2024) 100752, http://dx.doi.org/10.1016/j.padiff. 2024.100752.
- [30] S. Rana, R. Tabassum, R. Mehmood, E.M. Tag-eldin, R. Shah, Influence of Hall current & Lorentz force with nonlinear thermal radiation in an inclined slip flow of couple stress fluid over a Riga plate, Ain Shams Eng. J. 15 (1) (2024) 102319, http://dx.doi.org/10.1016/j.asej.2023.102319.
- [31] O.D. Makinde, On MHD heat and mass transfer over a moving vertical plate with a convective surface boundary condition, Can. J. Chem. Eng. 88 (6) (2010) 983–990. http://dx.doi.org/10.1002/cjce.20369.
- [32] K. Singh, S.K. Rawat, M. Kumar, Heat and mass transfer on squeezing unsteady MHD nanofluid flow between parallel plates with slip velocity effect, J. Nanosci. 2016 (1) (2016) 9708562, http://dx.doi.org/10.1155/2016/9708562.
- [33] K. Suneetha, S. Ibrahim, G.V.R. Reddy, A study on free convective heat and mass transfer flow through a highly porous medium with radiation, chemical reaction and soret effects, J. Comput. Appl. Res. Mech. Eng. 8 (2) (2019) 121–132, http://dx.doi.org/10.22061/jcarme.2017.2018.1175.
- [34] B.S. Goud, Y.D. Reddy, V.S. Rao, Thermal radiation and joule heating effects on a magnetohydrodynamic casson nanofluid flow in the presence of chemical reaction through a non-linear inclined porous stretching sheet, J. Nav. Archit. Mar. Eng. 17 (2) (2020) 143–164, http://dx.doi.org/10.3329/jname.v17i2.49978.
- [35] Y.-P. Lv, N. Shaheen, M. Ramzan, M. Mursaleen, K.S. Nisar, M. Malik, Chemical reaction and thermal radiation impact on a nanofluid flow in a rotating channel with Hall current, Sci. Rep. 11 (1) (2021) 19747, http://dx.doi.org/10.1038/ s41598-021-99214-v.
- [36] M. Hasanuzzaman, S. Akter, S. Sharin, M.M. Hossain, A. Miyara, M.A. Hossain, Viscous dissipation effect on unsteady magneto-convective heat-mass transport passing in a vertical porous plate with thermal radiation, Heliyon 9 (3) (2023) e14207, http://dx.doi.org/10.1016/j.heliyon.2023.e14207.
- [37] B.K. Jha, G. Samaila, Nonlinear approximation for buoyancy-driven mixed convection heat and mass transfer flow over an inclined porous plate with joule heating, nonlinear thermal radiation, viscous dissipation, and thermophoresis effects, Numer. Heat Transfer B 83 (4) (2023) 139–161, http://dx.doi.org/10. 1080/10407790.2022.2150341.
- [38] M.S. Ram, K. Spandana, M. Shamshuddin, S. Salawu, Mixed convective heat and mass transfer in magnetized micropolar fluid flow toward stagnation point on a porous stretching sheet with heat source/sink and variable species reaction, Int. J. Modelling Simul. 43 (5) (2023) 670–682, http://dx.doi.org/10.1080/ 02286203.2022.2112008.
- [39] P.M. Zar, B. Jalili, P. Jalili, D.D. Ganji, Thermal study of magnetohydrodynamic nanofluid flow and Brownian motion between parallel sheets, Int. J. Thermofluids 23 (2024) 100806, http://dx.doi.org/10.1016/j.ijft.2024.100806.
- [40] J.C. Maxwell, On the dynamical theory of gases, Philos. Trans. R. Soc. Lond. 157 (1867) 49–88.
- [41] Z. Abbas, M. Sajid, T. Hayat, MHD boundary-layer flow of an upper-convected Maxwell fluid in a porous channel, Theor. Comput. Fluid Dyn. 20 (2006) 229–238, http://dx.doi.org/10.1007/s00162-006-0025-y.

- [42] T. Hayat, R. Sajjad, Z. Abbas, M. Sajid, A.A. Hendi, Radiation effects on MHD flow of Maxwell fluid in a channel with porous medium, Int. J. Heat Mass Transfer 54 (4) (2011) 854–862, http://dx.doi.org/10.1016/j.ijheatmasstransfer. 2010.09.069
- [43] O. Ojjela, P.K. Kambhatla, N. Naresh Kumar, S.K. Das, Influence of cross-diffusion on slip flow and heat transfer of chemically reacting UCM fluid between porous parallel plates with Hall and ion slip currents, J. Comput. Eng. 2016 (1) (2016) 9160956, http://dx.doi.org/10.1155/2016/9160956.
- [44] N.P. Pai, B. Devaki, K.V.S. Sampath, P.G. Bhat, Analysis of magnetic effect on UCM fluid flow between a stationary and a moving plate, Eng. Lett. 32 (4) (2024).
- [45] J. Choi, Z. Rusak, J. Tichy, Maxwell fluid suction flow in a channel, J. Non-Newton. Fluid Mech. 85 (2-3) (1999) 165–187, http://dx.doi.org/10.1016/S0377-0257(98)00197-9
- [46] V. Aliakbar, A. Alizadeh-Pahlavan, K. Sadeghy, The influence of thermal radiation on MHD flow of maxwellian fluids above stretching sheets, Commun. Nonlinear Sci. Numer. Simul. 14 (3) (2009) 779–794, http://dx.doi.org/10.1016/j.cnsns.2007.12.003.
- [47] S. Mukhopadhyay, M.G. Arif, M.W.A. Pk, Effects of transpiration on unsteady MHD flow of an upper convected Maxwell (UCM) fluid passing through a stretching surface in the presence of a first order chemical reaction, Chin. Phys. B 22 (12) (2013) 124701, http://dx.doi.org/10.1088/1674-1056/22/12/124701.
- [48] C. Fetecau, R. Ellahi, S.M. Sait, Mathematical analysis of Maxwell fluid flow through a porous plate channel induced by a constantly accelerating or oscillating wall, Mathematics 9 (1) (2021) 90, http://dx.doi.org/10.3390/ math9010090.
- [49] A. Khan, I.A. Shah, A. Khan, I. Khan, W.A. Khan, Numerical investigation of MHD Cattaneo-Christov thermal flux frame work for Maxwell fluid flow over a steady extending surface with thermal generation in a porous medium, Int. J. Thermofluids 20 (2023) 100418, http://dx.doi.org/10.1016/j.ijft.2023.100418.
- [50] S. Zeb, Z. Ullah, H. Urooj, I. Khan, A. Ganie, S. Eldin, Simultaneous features of MHD and radiation effects on the UCM viscoelastic fluid through a porous medium with slip conditions, Case Stud. Therm. Eng. 45 (2023) 102847, http: //dx.doi.org/10.1016/j.csite.2023.102847.
- [51] S. Zeb, A. Adnan, W. Ahmad, S. Ahmad, I. Samuilik, Thermal stratification and heat generation/absorption impacts on stagnation point flow of MHD UCM fluid through a permeable medium, Partial. Differ. Equations Appl. Math. 10 (2024) 100692, http://dx.doi.org/10.1016/j.padiff.2024.100692.
- [52] J.-H. He, Homotopy perturbation technique, Comput. Methods Appl. Mech. Engrg. 178 (3) (1999) 257–262, http://dx.doi.org/10.1016/S0045-7825(99)00018-3
- [53] J.-H. He, A coupling method of a homotopy technique and a perturbation technique for non-linear problems, Int. J. Non-Linear Mech. 35 (1) (2000) 37–43, http://dx.doi.org/10.1016/S0020-7462(98)00085-7.
- [54] J.-H. He, Homotopy perturbation method: a new nonlinear analytical technique, Appl. Math. Comput. 135 (1) (2003) 73–79, http://dx.doi.org/10.1016/S0096-3003(01)00312-5.
- [55] E. Babolian, A. Azizi, J. Saeidian, Some notes on using the homotopy perturbation method for solving time-dependent differential equations, Math. Comput. Modelling 50 (1-2) (2009) 213-224, http://dx.doi.org/10.1016/j.mcm.2009.03.
- [56] P.L. Sachdev, N.M. Bujurke, N.P. Pai, Dirichlet series solution of equations arising in boundary layer theory, Math. Comput. Modelling 32 (9) (2000) 971–980, http://dx.doi.org/10.1016/S0895-7177(00)00183-7.
- [57] M. Turkyilmazoglu, An analytic shooting-like approach for the solution of nonlinear boundary value problems, Math. Comput. Modelling 53 (9–10) (2011) 1748–1755, http://dx.doi.org/10.1016/j.mcm.2010.12.053.
- [58] M. Turkyilmazoglu, The Airy equation and its alternative analytic solution, Phys. Scr. 86 (5) (2012) 055004, http://dx.doi.org/10.1088/0031-8949/86/05/ 055004
- [59] N. Abdelhalim, R. Imad, B. Abdelouahab, Application of the homotopy perturbation method for differential equations, WSEAS Trans. Syst. 22 (2023) http://dx.doi.org/10.37394/23202.2023.22.32.
- [60] K.V.S. Sampath, B. Devaki, P.G. Bhat, N.P. Pai, K.R. Vasanth, K.G. Kumar, Analysis of flow and heat transfer characteristics of ethylene glycol-based magnetite nanoparticles squeezed between parallel disks with magnetic effect, J. Therm. Anal. Calorim. 149 (21) (2024) 12219—122302, http://dx.doi.org/ 10.1007/s10973-024-13481-1.
- [61] M. Abbasi, M. Khaki, A. Rahbari, D. Ganji, I. Rahimipetroudi, Analysis of MHD flow characteristics of an UCM viscoelastic flow in a permeable channel under slip conditions, J. Braz. Soc. Mech. Sci. Eng. 38 (2016) 977–988, http: //dx.doi.org/10.1007/s40430-015-0325-5.
- [62] M. Ali, T. Chen, B. Armaly, Natural convection-radiation interaction in boundary-layer flow over horizontal surfaces, AIAA J. 22 (12) (1984) 1797–1803, http://dx.doi.org/10.2514/3.8854.